Effect of diatomite addition on crystalline phase formation of TiO 2 and photocatalytic degradation of MDMA

Leila Bengotni, Belhadj Trari, Bénédicte Lebeau, Laure Michelin, Ludovic Josien, Abdelkader Benguedach, Rachida Hamacha

Effect of diatomite addition on crystalline phase formation of TiO2 and photocatalytic degradation of MDMA

Leila Bengotni[1], Belhadj Trari[2], Bénédicte Lebeau[3,4], Laure Michelin[3,4], Ludovic Josien[3,4] Abdelkader Benguedach[1], Rachida Hamacha[1,*]

[1]Laboratoire de Chimie des Matériaux L.C.M, Université Oran1 Ahmed Ben Bella, BP 1524, El-Mnaouer, 31000 Oran, Algérie.
[2]Laboratoire de chimie organique, Université des Sciences et de la Technologie d'Oran Mohamed-Boudiaf (USTO), El Mnaouer, BP 1505, Bir El Djir 31000, Oran Algérie
[3]Université de Haute Alsace (UHA), CNRS, Axe Matériaux à Porosité Contrôlée (MPC), IS2M UMR 7361, F-68100 Mulhouse, France.
[4]Université de Strasbourg, F-67000 Strasbourg, France
* Email address: rachidahamacha@gmail.com

In the present study, titanium dioxide nanoparticles (TiO_2NPs) were immobilized on Algerian diatomite surface by simple sol-gel method for improving the photocatalytic efficiency of TiO_2. A series of composites TiO_2/Diatomite (TiD) was synthesized with different amounts of diatomite and TiO_2 NPs composed of mixed rutile/anatase phase for the photodegradation under UV- irradiation of 3,4-methylenedioxymethamphetamine (MDMA), otherwise known as Ecstasy. This illicit drug is the most consumed among adolescents and identified in wastewater effluents. The effect of diatomite addition on formation of crystalline phase, crystallite size and porosity was investigated. The results showed that the rutile/anatase phase ratio in TiO_2NPs can be controlled through the diatomite addition. Morphological and structural characterizations of the prepared composites have been carried out by using X-ray diffraction (XRD), X-ray Fluorescence (XRF), Nitrogen sorption at 77K, scanning and transmission electron microscopy (SEM and TEM, respectively), energy dispersive X-ray spectroscopy (EDS) and Ultra-Violet reflectance diffuse spectroscopy. All prepared composites TiD displayed a remarkable enhancement of the photocatalytic activity compared to pure commercial and synthesized TiO_2. The composite which contains a mixed phase rutile/anatase (at 42:58 weight or molar ratio) and SiO_2 content of 20 wt.% exhibits the best and the highest photocatalytic activity in the degradation of MDMA.

Introduction

The consumption of illicit drugs has been sharp increasing in worldwide [1], hence recently several studies focused on the quantification of these important contaminants in wastewater effluents and showed that amphetamine, cocaine, MDMA (commonly called Ecstasy) and methamphetamine [2] are the most abused and detected illegal drugs. According to wastewater analysis there is an increase of MDMA in residues compared to previous years [3].
The majority of this emerging pollutant cannot be completely removed in wastewater treatment plants. Thus, most of the analysis wastewater showed that removal efficiency of MDMA was about 32-50 % [4] due to its stability in wastewater [5-8]. This confirms what has already been pointed out that illicit drugs and in particular MDMA are able to get in the groundwater and surface water and can pose a risk to the animal and human health, environmental quality and ecosystems [9-11]. Until now, very few studies have investigated the removal and degradation of illicit drugs [12].
In the present work, heterogeneous photocatalysis technology is used for the photodegradation of MDMA. This technique is widely employed for wastewater treatment, air purification and decomposition of emerging contaminants resistant to conventional treatment technique [13-16]. Some of these authors made detailed mechanism of the photocatalysis reaction by exploring the species implicated in the photocatalytic act and which are responsible of either oxidation or reduction of the pollutant [14-16].
It is based on the excitation of semiconductor by light, forming the pair electron (e-)/hole (h+), which can directly photodegrade and mineralize organic compounds or produce free radicals (hydroxyl $OH^{\cdot}$ and peroxide radicals ($O_2^{\cdot-}$)) with high oxidizing properties [17,18].
Actually, titanium dioxide (TiO_2) has been widely studied and used as an excellent photocatalyst due its high photocatalytic performance, chemical and biological stability, non-toxicity, inertness and low cost [19-20]. It is also used in various applications [21] such as anticorrosion and self-cleaning surfaces [22]. TiO_2 has three polymorphs: anatase, rutile (tetragonal system) and brookite (orthorhombic system) [23]. The rutile crystalline phase is the most common and most thermodynamically stable phase [24]. For many authors, anatase phase is more photocatalytically active than rutile and brookite due to its lower crystallite size and wider band gap energy. The electronic band gap between conduction and valence bands is reported at 3,0 eV for rutile and 3,2 eV for anatase [25].
On the other hand, the agglomeration of TiO_2Nps in suspension and their low surface area [23] decreases significantly its photocatalytic performance; hence the immobilization of TiO_2 particles on porous materials was the best solution to this problem. Variety of supports have been used such as silica mesoporous SBA-15 [26], diatomite [27, 28], montmorillonites [29], zeolite [30], kaolinite [31] and perlite [3].
Mesoporous Silica (SiO_2) has attracted much attention as a catalyst support due to its high specific surface area (SSA) which improved the adsorption capacity of pollutants [33,34] . Previous studies have proved that silica plays an active role in the TiO_2 photocatalytic efficiency compared to pure TiO_2 by providing and increasing hydroxyl groups

on the surface of TiO_2 [35]. Others recent studies [36-38] revealed that SiO_2 addition delayed the anatase to rutile transformation in TiO_2 and contributed to stabilize the anatase phase [39].

In this study, Algerian diatomite was chosen as natural and porous mineral support for TiO_2Nps, due to its abundance and low cost, high porosity, low density, low thermal conductivity and chemical inertness [40,41]. Besides it is a fine porous and siliceous rock consisting mainly of amorphous silica (SiO_2, nH_2O).
The majority of studies dealing with the synthesis of TiO_2 NPs supported on SiO_2 for photocatalysis found that only anatase crystalline phase was formed [42], which has the best photocatalytic activity compared to the others TiO_2 crystalline phase [41-44]. Recently, several theoretical [45] and experimental studies [42-45] showed that mixed phases (rutile/anatase) [50] and (anatase/brookite) [51] exhibit higher photocatalytic activity than pure anatase or rutile phase due to the interface rutile/anatase heterojunction which reduces the electron (e^-)-hole(h^+) recombination [52]. Y. Wei [53] proved using *ab initio* calculation that the lifetime of charges separation (e^-, h^+) in TiO_2 mixed phase is longer than in pure rutile and anatase phases. It was also found that a ternary mixture of anatase, rutile and brookite phase inhibits the recombination of charges pairs by capturing the electrons [54-55].
Under the same concept, this study aims to prepare different composites materials TiO_2/diatomite with different amounts of Algerian diatomite and TiO_2Nps with different anatase /rutile ratio in order to optimize the photocatalytic performance for MDMA degradation in water. The effect of diatomite addition on the nature of crystalline phase formed using a simple sol-gel method was investigated for the first time in order to control the ratio anatase/rutile. Other parameters such as surface area, TiO_2 crystallite size and composition of mixed anatase/rutile phase were also studied. The photocatalytic activity of the obtained composites was evaluated in the degradation of MDMA.

Experimental

Diatomite pretreatment.

The diatomite (denoted as Dt) used in this work was collected from west of Algeria (Sig). The predominant mineralogical components of Dt are SiO_2 (63%), CaO (19%), Al_2O_3 (4%) and other oxides.
The raw diatomite has been milled to grains of less than 0.5 mm and undergoes an acid and thermal pre-treatment to purify it and remove organic matter and traces of carbonate that block the pores before combined with TiO_2.
The acid treatment of diatomite was carried out by different concentrations of sulfuric acid (2M, 3M and 4M) with *liquid*-to-*solid ratio (ml/g) of* (20:1).
10 grams of crude diatomite were mixed with 200 ml of sulfuric acid and heated at 100 ° C for 3 hours with moderate agitation under reflux conditions. Then, obtained samples were washed several times by deionized water until neutralization and dried at 100 °C for 12 hours. Finally, the thermal treatment was performed at 550 °C in air for 3 hours with heating rate of 5 °C/min. The samples of treated diatomite were denoted by $Dt_{(2M)}$, $Dt_{(3M)}$ and $Dt_{(4M)}$.

Preparation of TiO_2/diatomite composites

Titanium (IV) n-butoxide (AlfaAesar, 99%) noted (TBut) was chosen as the TiO_2 precursor. Nitric acid (HNO_3 65%), ethanol absolute (99%), sulfuric acid (H_2SO_4) were purchased from MERCK, while acetonitrile was purchased from VWR Chemicals PROLABO.
Pure MDMA used for the photocatalytic study was obtained from the Scientific Police Regional Laboratory (Oran) of Algeria.
Different amounts of the purified diatomite were mixed with 20 ml of deionized water and 5 ml of absolute ethanol, and stirred during 30 min. The pH value of the solution was adjusted at 2 by the addition of nitric acid (HNO_3) to obtain the first solution (S1). Then 5 ml of (TBut) dissolved in 20 ml of absolute ethanol was added drop by drop to the S1 solution under vigorous stirring at room temperature for 3 hours. The final mixture was aged without stirring for further 96 h. The obtained white precipitate was recovered by filtration, washed several times with deionized water, and dried at 80°C for 24 h.
Finally, the resulting powders were calcined at 500ºC (10 °C/min) for 120 min in muffle furnace (in air).
Based on the results of the X-ray fluorescence technique (XRF), the content of SiO_2 in prepared composites was estimated to be 13, 20, 29, 34, 40, 48, 53 and 68 wt.% corresponding at different weight of diatomite (0.2, 0.4, 0.6, 0.8, 1, 1.2, 1.4 and 1.6 g, respectively), and the corresponding composites are represented as TiD(x %), where x is the weight percentage of SiO_2.
For comparison purposes, pure TiO_2 was also synthesized in mixed rutile/anatase phase and pure anatase phase with and without addition of catalyst (HNO_3), respectively, by the same process as described above, except that diatomite was not added.

Characterization techniques and methods

Materials

In order to determine the chemical composition of the crude diatomite, diatomite treated at different concentrations and the synthesized composites, X-ray fluorescence technique (XRF) analyzes was performed using a PANalytical spectrometer model Zetium.
The XRD analysis of the prepared samples was done using a Bruker D2 Phaser 2nd Gen diffractometer with Cu anode (λ=1.5406 nm), and data were taken in the 2θ range from 10° to 70° with a step of 0.1972°.
The morphology of prepared samples was observed using a Philips model XL30 scanning electron microscope (SEM-FEG) equipped with an energy dispersive X-ray spectroscopy (EDS) equipment. Transmission Electron Microscopy (TEM) observations were performed using a Jeol ARM-200F microscope working at 200kV.

The concentrations of MDMA were determined by High Performance Liquid Chromatography HPLC 1110 (Agilent Technologies) with a linear photodiode array detector (HPLC-DAD) at 230 nm, isocratic mode, reversed-phase Zorbax Eclipse Plus® C18 (4.6 x 150 mm, 5.0 µm) column, injected volume 5 µL, column temperature of 30 °C and a flow of mobile phase Acetonitrile : water (80:20 v/v) at 1.0 mL/min.
Brunauer-Emmet-Teller (BET) and Barrett-Joyner-Halenda (BJH) methods were also used for determining the specific surface area (SSA) and the total pore volume distribution from nitrogen adsorption/desorption at 77K on outgassed samples (15 h at 150°C under 10^{-3} mbar vacuum) with a Micromeritics sorptometer model Tristar.

Methods

The weight or molar fractions of rutile (%R) and anatase (%A) in prepared composite were determined by XRD analysis according to the method described by Spurr and Meyer equation [56],
As follows:

$$\% \ anatase = \frac{1}{1+1.26\left(\frac{I_R}{I_A}\right)}$$

Where, I_R and I_A are the intensities of maximum rutile phase peak (110) and maximum peak of anatase phase (101) observed at 2θ= 27.5° and 2θ=25.39°, respectively. The trace amount of brookite was negligible. The 1.26 value is the scattering coefficient.
The crystalline sizes of TiO_2Nps were determined using the Scherrer equation [57], as follows:

$$D(nm) = \frac{K\lambda}{\beta \cos\theta}$$

Where *D* is the crystalline size (nm), λ is the wavelength of the X-ray radiation (CuKα = 0.154056 nm), K is a shape factor (in this work K = 0.9), θ the Bragg's angle and β is the peak full width measured at half of the maximum intensity (FWHM) for the main diffraction peak.
The values of the band gap energy (Eg) were calculated using the Kubelka-Munk method [30], which consists of graphing the function $[F(R_\infty)hv]^{1/2}$ versus energy ($h\upsilon$) for an indirect photoatalyst. It was obtained by extrapolating the linear part of the plots corresponding to the intersection of the vertical parts and photon energy axis (horizontal part).
$F(R_\infty) = K/S$ where *K* is the absorption coefficient, *S* is the scattering coefficient, *h is* Planck's constant and *υ is* light frequency.

Photocatalytic experiments

Photocatalytic experiments were performed using an ultraviolet irradiation source (lamp F18 W/T8 black light tube λ=368 nm) placed at a distance of approximately 15 cm from the solution. Constant agitation was assured by means of a magnetic stirrer.
Photocatalytic degradation studies were performed by mixing 1g of all prepared photocatalyst powder dispersed into 1 L of MDMA aqueous solutions at an initial concentration of 10 mg/L. The mixture was first placed in the dark for 60 min under stirring to reach adsorption equilibrium, and then irradiated. Aliquots taken at different irradiation times were centrifuged and filtered to remove the particles of photocatalyst. The concentration of the photodegraded MDMA was determined using HPLC-DAD at the maximum absorption wavelength of 230 nm.
The MDMA percentage adsorbed on the composite in the dark and the photocatalytic degradation rate of MDMA under UV illumination were calculated by the following equation:

$$(removal\ rate\ \%) = \frac{(C_0 - C_t)}{C_0} * 100$$

Where C_0 and C_t are the initial and the residual concentrations of MDMA separated at different irradiation times, respectively.

Results and discussion

Structural analysis of prepared samples

Diatomite characterizations.

In Fig. 1 are displayed the XRD spectra of raw and acid treated diatomites. XRD analysis of the diatomite before and after thermal and acid treatment showed that the main chemical composition of the treated diatomites ($Dt_{(2M)}$, $Dt_{(3M)}$ and $Dt_{(4M)}$) is amorphous silica (XRD halo centered at approximately 2θ=22°), quartz(Q)[54], and small amount of muscovite (M)(Fig. 1).showed that the main chemical composition of the treated diatomites ($Dt_{(2M)}$, $Dt_{(3M)}$ and $Dt_{(4M)}$) is amorphous silica (XRD halo centered at approximately 2θ=22°), quartz(Q)[54], and small amount of muscovite (M)(Fig. 1).

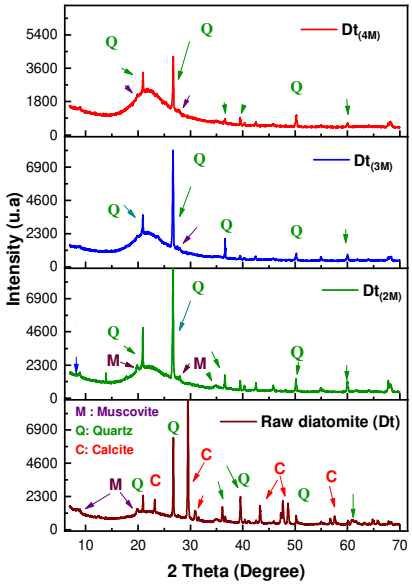

Fig. 1. XRD patterns of raw diatomite (Dt), and treated diatomites with sulfuric acid at different concentration $Dt_{(2M)}$, $Dt_{(3M)}$ and $Dt_{(4M)}$

After treatment with increased sulfuric acid concentration the intensity of quartz characteristic peaks observed at 21° and 26.7° was decreased, and an amorphous phase of SiO_2 was observed whereas calcite was eliminated in all cases.
Chemical compositions and textural properties from nitrogen adsorption/desorption analysis of the purified and raw diatomite are reported in **Table 1.** It could be deduced that the thermal and acid treatment at different concentrations lead to an increase in the SSA and silica content of the diatomite with increasing H_2SO_4 acid concentration. The significant increase from 27 m^2/g (crude diatomite) to 71 m^2/g $Dt_{(4M)}$ and from 63.7wt.% to 97.3 wt.% of SiO_2 is due to the elimination of significant amount of carbonates (19%) and some alumina Al_2O_3(4%) that partially block the pores without modifying its morphology.

Table 1. Chemical composition and physical properties of natural and purified diatomite at different concentration of sulfuric acid 2M, 3M and 4M

Samples	SiO_2	Al_2O_3	CaO	Fe_2O_3	S_{BET} (m^2/g)
Dt	63.7	4.01	18.2	2.08	27
$Dt_{(2M)}$	91.5	3.64	16.7	1.48	28
$Dt_{(3M)}$	94	3.41	0.22	0.47	67
$Dt_{(4M)}$	97.3	2.12	-	-	70

Photocatalysts characterizations.
The XRD diffraction of pure TiO_2 powders prepared using a strong acid media (pH is about 2) (Fig. 2), showed that TiO_2 exhibits a mixture of a predominantly rutile phase (85%) and minor anatase phase (15%), identified by the presence of intense diffraction peaks of rutile phase (2ϑ = 27.4°, 36°, 39.3°, 41.2°, 44°, 54.3° , 56.8° , 62.9°, 64° and 69°) while the anatase phase is evidenced by only one peak with very low intensity at 25.3°.

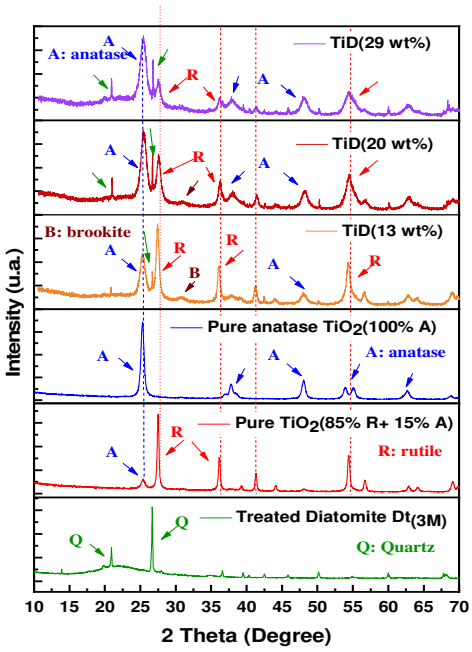

Fig. 2 XRD patterns of prepared pure anatase TiO_2 (100 wt. %), mixed phase TiO_2 (rutile:anatase is 85:15) and composite containing less than 34 wt.% of SiO_2

Whereas, pure anatase TiO_2 was obtained by the same process without adding the acid catalyst and is characterized by peaks at 2ϑ = 25.3°, 37.8°, 37.8°, 38.4°, 48°, 53.8° , 55.1° , 62° and 68.8°, due to the hydrolysis pH value which has an important effect on the crystallographic structure of TiO_2. Similar results also showed that at low pH mixed anatase/rutile phase was formed [50, 59-60]. In addition, Andersson et al reported that the formation of rutile and anatase NPs depends on the type of acid used and its concentration [61].

For the synthesis of all composites TiD(SiO_2 %), only the diatomite treated with 3M sulfuric acid was chosen as the support for the TiO_2NPs, because it has a high content of silica (94 wt.% of SiO_2) and specific surface area (S_{BET} of 67 m^2/g).

X-ray diffraction (XRD) patterns of composites synthesized with small amounts of diatomite (less than 34 wt.% of SiO_2) are presented in Fig. 2. Fig. 3 shows the XRD patterns of other composites containing more than 34 wt. % of SiO_2.

It can be seen that when the amount of added diatomite is smaller than 0.8 g (up to 34 wt. % of SiO_2 content), both anatase (TiO_2, JCPDS card no. 21-1272) and rutile phases (TiO_2, JCPDS card no. 21-1276) are formed with different proportions with the presence of minor trace of brookite phase (TiO_2, JCPDS card no. 29-1360). The latter is observed at 31° (very low intensity) solely for TiD(13%) and TiD(20%) composites (Fig. 3). From Table 2 it can be seen that a mixture of 39 wt. % anatase and 61 wt.% rutile was found for TiD(13%), which contains a lower amount of diatomite, while for TiD(20%), TiD(29%) and TiD(34%) composites, 54 wt.%, 63 wt.% and 90 wt.% of mass fraction of anatase were obtained, respectively.

It can be seen also from Fig. 2 that the intensity of rutile (at 27.5°) was decreased significantly with increasing diatomite amount or silica content in composites until 34 wt.% of SiO_2. It is deduced that the presence of diatomite in the composite at low amount (less than 34 wt.% of SiO_2) affects the formation of rutile phase and favors the anatase phase formation.

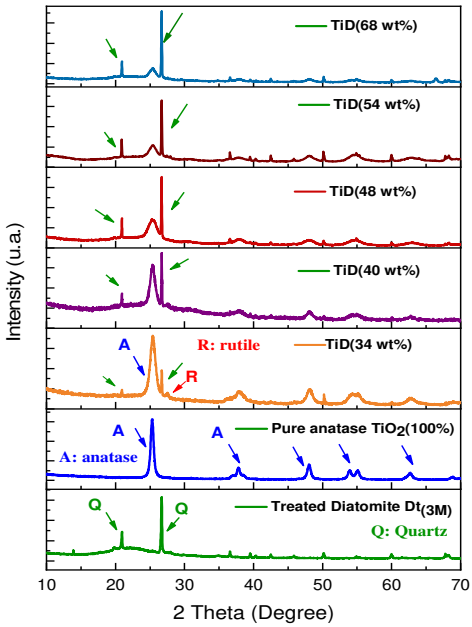

Fig. 3 XRD patterns of prepared pure anatase TiO_2 and composite containing more than 34 wt.% of SiO_2.

Fig. 3 shows that a pure anatase phase can be observed when the silica content is more than 34 wt.%. The major XRD peaks can be attributed to anatase (25.4°, 37.8°, 48°, 53.8°, 55.1° and 62°) with two characteristic peaks at 2θ = 21.4° and 26.7 ° related to quartz (SiO_2). No peaks associated to the brookite phase were detected in this kind of composite.

This result is in agreement with the work of M. Hirano [42], which showed that anatase phase was directly prepared from solutions of $TiOSO_4$ in the presence of 48.2 mol.% SiO_2 using tetraethylorthosilicate as silica precursor under hydrothermal conditions at 200 °C, and that the as-prepared solid displayed more enhanced phase stability and photocatalytic activity than pure TiO_2 anatase.

In Fig. 4 is illustrated the relationship between the weight % of rutile / anatase phases and SiO_2 content in synthesized composites. It seems that the addition of certain amount of diatomite inhibits the formation of rutile phase and favors the growth and formation of anatase. When the diatomite SiO_2 content was more than 34 wt.%, only anatase phase was formed with small particle size (Fig. 5) but when pure TiO_2 was synthesized with the same experimental condition rutile phase was predominantly formed with minor content of anatase (Fig. 2 and Fig. 3). This is in agreement with similar work carried out by D.M. Tobaldi [62] who obtained mixed phase by thermal treatment of two commercial titania powders and a silica powder, and reported that silica addition affected crystallite size, SSA and TiO_2 phase composition.

D.M.Tobaldi [62] have also found that rutile crystallite size decreases with the increasing amount of SiO_2 added to P25 heated at 1000°C. As illustrated in Table 2, the crystallite size of anatase phase remains small and quasi constant (8-9 nm) when small amount of diatomite was added, but vary slightly when SiO_2 proportion is more than 34 wt.% to reach the range of 5 –8 nm. It clearly seems that crystallite size depends on the SiO_2 content in diatomite (Fig. 5).

The crystallite sizes of anatase and rutile as calculated by the Scherrer equation are reported in Table 2. It is seen that the crystallite size of TiO_2 depends strongly on the diatomite content in composites. For pure TiO_2, the crystallite size of anatase phase is about 15 nm and 30.9 nm for rutile phase, when diatomite was added this value decreases with increasing diatomite amount from 30.9 nm (pure TiO_2) to 12 nm for rutile crystalline structure.

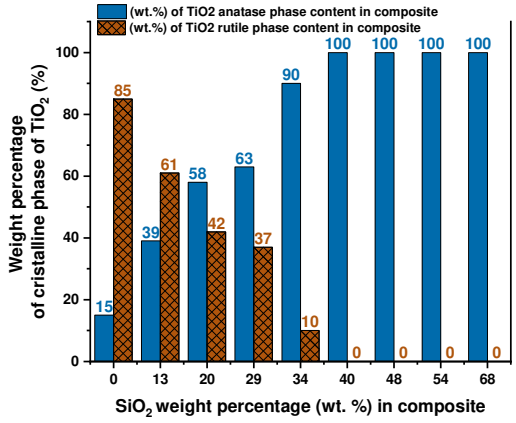

Fig. 4 Relationship between weight percentage of TiO_2 anatase phase and SiO_2 content in the composites.

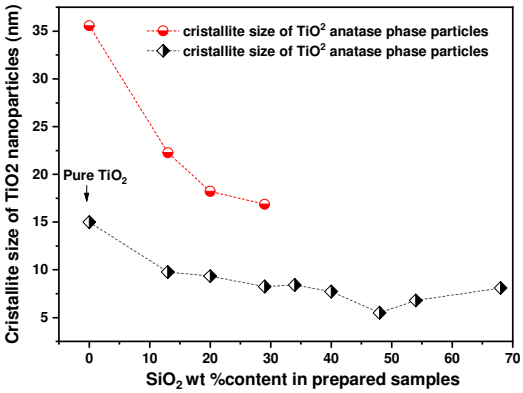

Fig. 5 Relationship between crystallite size of TiO_2 NPs and SiO_2 content in prepared composites.

Textural characterization (Nitrogen sorption). Fig. 6 displays the N_2 adsorption–desorption isotherms of pure TiO_2 and composites containing mixed TiO_2 phases while Fig. 7 shows isotherms of crude diatomite, treated diatomite $Dt_{(3M)}$ and composites prepared with TiO_2 containing only anatase phase. As seen from the Fig. 6 and 7, the N_2 adsorption–desorption isotherm of raw diatomite corresponds to type II indicating a non porous structure in the limit of technique detection (small pores with average size < 20 nm). After the removal of impurities and minerals by acid and thermal treatment, treated diatomite exhibited typical characteristic of type IV with distinct type H1 hysteresis loop, indicating of mesoporous material (Fig. 7).

The apparition of mesopores can be related to the increase of amorphous SiO_2 phase as observed by XRD. Acid treatment has removed mineral impurities and thus opened blocked mesopores [63]. Silicon species could also be leached out from diatomite surface by acid treatment and precipitate into mesoporous silica gel [64].

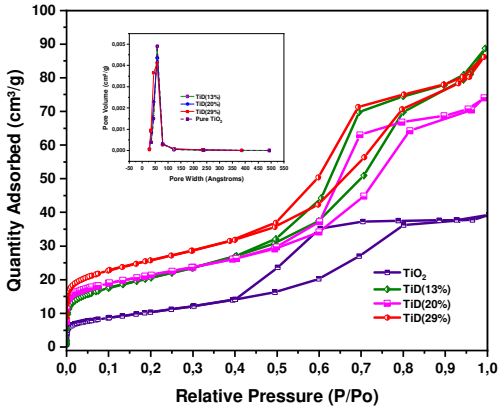

Fig. 6 N_2 adsorption-desorption isotherms and BJH pore size distribution plots of pure TiO_2 and composite containing less than

Table 2. Characterization of the synthesized samples

Samples TiD(SiO_2 wt.%)	**SiO_2** wt.%[a]	TiO_2 wt.%[a]	**Rutile** (wt.%)[b]	**Anatase** (wt.%)[b]	**Crystalline size**(nm) [c]		**SSA BET**[d] (m^2/g)	**Pore size**[e] (nm)	**Total pore volume**[d] (cm^3/g)	**Bandgap energy**(eV)
$Dt_{(3M)}$	94	-	-	-	Rutile (R)	Anatase (A)	67	3.4	0.123	
Pure TiO_2		100	85	15	30.9	15	42.4	4.1	0.061	2.88
TiD(13 %)	13	85	61	39	17.6	9.8	67.0	6.2	0.122	2.91
TiD(20 %)	20	77	42	58	13.1	9.3	72.0	5.9	0.137	2.93
TiD(29 %)	29	68	37	63	13.1	8.4	79.2	5.8	0.126	2.89
TiD(34 %)	34	62	10	90	12.2	8.2	82.4	4.7	0.145	3.1
TiD(40 %)	40	56	-	100	-	7. 7	81.4	4.6	0.137	2.98
TiD(48 %)	48	42	-	100	-	5.6	133	6.7	0.244	2.96
TiD(54 %)	56	39	-	100	-	6.8	87.8	4.4	0.137	3.04
TiD(68 %)	68	27	-	100	-	8.1	104	5.6	0.169	3.17

[a] Determined by XRF
[b] Calculated from the X-ray diffraction peaks
[c] Determined by XRD using the Scherrer equation
[d]Calculated from nitrogen adsorption–desorption isotherms using BET equation.
[e] Calculated from the adsorption branch of the isotherm using Barret–Joyner–Halenda (BJH) method calculated from nitrogen adsorption–desorption isotherms at P/P° = 0.95

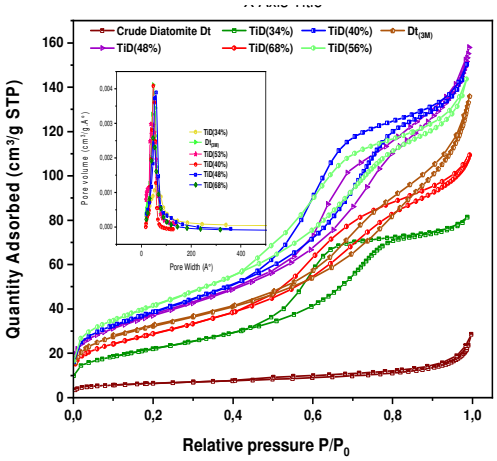

Fig. 7 N_2 adsorption-desorption isotherms and BJH pore size distribution plots of crude diatomite, treated diatomite $Dt_{(3M)}$ and composite containing more than 34 wt.% of SiO_2

All prepared composites maintain a type IV isotherm according to the IUPACs classification [65] with a hysteresis loop of H2 type in the relative pressure (P/P_0) range of 0.4~0.9, indicating the formation of mesoporous structures [66].
The textural properties of all samples given in Table 2 prove that the immobilization of TiO_2 NPs on the diatomite surface greatly enhanced both SSA and total pore volume of TiD composites compared to pure TiO_2 (42.4 m^2/g; 0.0607 cm^3/g) which possesses lower SSA and pore volume due to the aggregation of NPs with larger size and to diatomite (SSA of 67 m^2/g). The SSA and total pore volume increase with increasing SiO_2 content in diatomite, until it reaches a maximum of 133 m^2/g and 0.244 cm^3/g, respectively, for the composite containing 48 wt.% of SiO_2. The latter is characterized by the smallest crystallite

size of TiO_2 particles (5 nm) uniformly dispersed on diatomite surface and mesoporous structure. The SSA values will decrease when SiO_2 content (wt.%) is greater than the TiO_2 ones.
The pore size distributions were obtained, using the BJH method applied on the desorption branch (Figs 6 and 7). It can be clearly seen that the prepared samples have large pore size (between 4.5 and 6 nm) with wide pore size distribution.

Photocatalysts morphology.
The SEM images of Dt(3M) reveal that the diatomite has porous structure with various types of morphology (Fig. 8b, f and j) and different shapes. It has circular morphology (disc-like shape) with round, uniform and regular pores, rectangular shapes are also observed with pore like honeycomb.

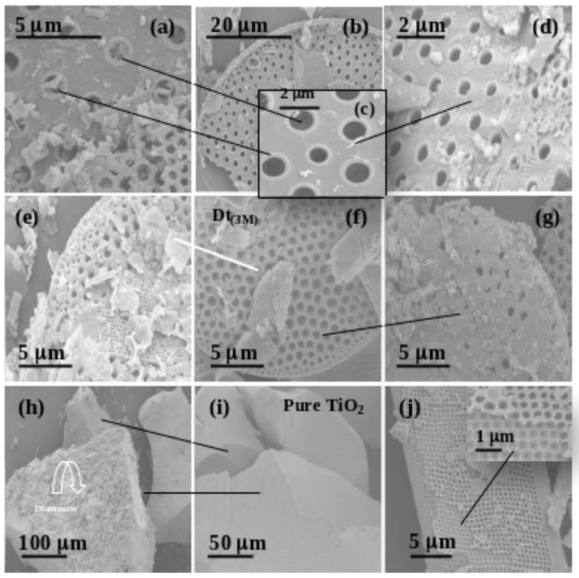

Fi crude diatomite;(c) : TiD(68%); (d) : TiD(53%); (e): T (20 wt. %), (i): Pure TiO_2

The mains pore structure of $Dt_{(3M)}$ is in range of 0.3-1.23 µm (macropores). Smaller pores were also observed with small fragments (broken diatom).
The morphology of pure TiO_2 containing 85 wt.% rutile and 15 wt.% anatase as characterized by TEM, is shown in Fig. 9.
It can be observed the formation of agglomerated TiO_2 NPs with irregular shape due to the mixture of major rutile phase and anatase phase (see Fig. 9). Some particles corresponding to rutile phase have elongated and ovoid shape with a size of about 15-50 nm length and 20–30 nm in width. The smaller particles with an average size less than 10 nm correspond to anatase phase with spherical form, as it was confirmed from crystalline size using XRD analysis (Table. 2).

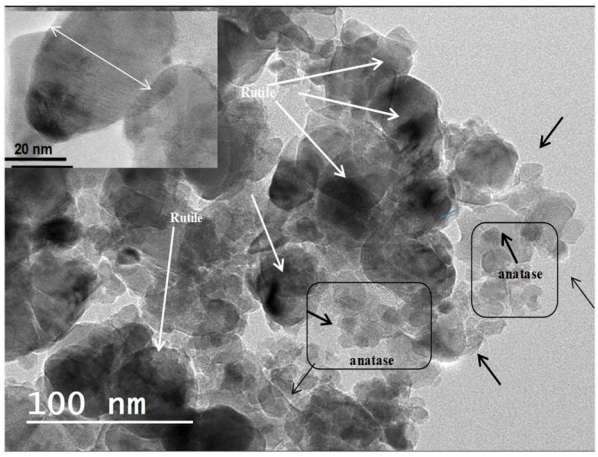

Fig. 9 TEM micrograph of pure prepared TiO_2 containing 85% rutile and 15% anatase

After adding different amount of diatomite (Fig.8 (a, c, d, g and e), we can observe uniform dispersion of TiO_2 particles on the surface and in pores of diatomite. The SEM images of TiD(29%), TiD(34%), TiD(48%) and TiD(40%) composites show a weak agglomeration of TiO_2NPs which is in agreement with the observed increase of SSA revealed by nitrogen sorption analysis and the grain size decrease when SiO_2 content increases. On the other hand, the SEM images of

TiD(13%) and TiD(20%) composites show the formation of agglomerates of TiO_2NPs due to the small amount of diatomite, which covered almost completely the diatomite surface (Fig. 8 (h) and Fig. 10).
In Fig. 10 is displayed the EDX elemental mapping images of TiD(20%), TiD(34%), and TiD(48%). One can clearly see the uniform distribution of Si, Ti and O elements on the surface of prepared composites, indicating a weak agglomeration of TiO_2NPs that could favor a good photocatalytic performance in MDMA photodegradation.

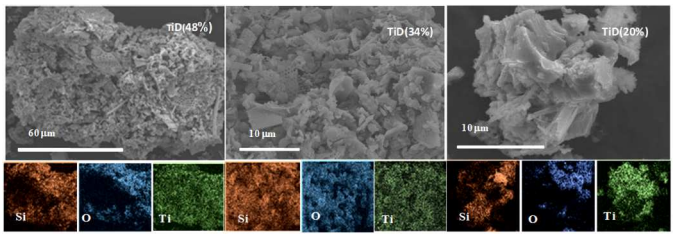

Fig. 10 SEM images and corresponding EDX Si, O, Ti element mappings of prepared composites: TiD(20%), TiD(34%) and TiD(48%)

UV-vis Diffuse Reflectance Specta (DRS) analysis

The optical absorption properties of synthesized photocatalyst was analyzed by using UV-Visible diffuse reflectance spectra (DRS), as shown in Figure 16, All composite prepared with different amounts of diatomite exhibited strong absorption in the UV light region in a range between 250-400 nm. It can also be seen that the composites containing up to 54 wt % of SiO_2 have stronger absorption intensity than pure TiO_2 between 250-380 nm. Thus, the TiD(48%) composite which has the best photocatalytic activity and where only anatase phase was formed showed the highest absorption.
Around 400 nm the composite containing mixed phase and small content of SiO2 exhibited a good light absorption compared to other composite. On the other hand, pure TiO_2 prepared without adding diatomite showed a weak absorption intensity in visible light region (at above 400 nm) and a slight blue shift was observed. This may be attributed to their mixed phase (anatase-rutile composition) which affect the nanoparticles size (Fig.5) and diatomite content (presence of TiO_2-SiO_2 mixed oxide junction). This results were confirmed by band gap energy values calculated according to the Kubelka-Munk method (Fig.12 and Table.2) which increase from 2.88 eV (pure TiO_2) to 3.17 eV (DTi(68%)). In figure 11 it is showed that when the diatomite is added the band gap energy (Eg) of composite increases with increasing diatomite amount. Thus the composite containing small amount of diatomite and (anatase-rutile) mixed phase show a higher UV light absorption and low values of Eg which could produce more photo-generated electron-hole pairs, resulting in high photocatalytic activities.

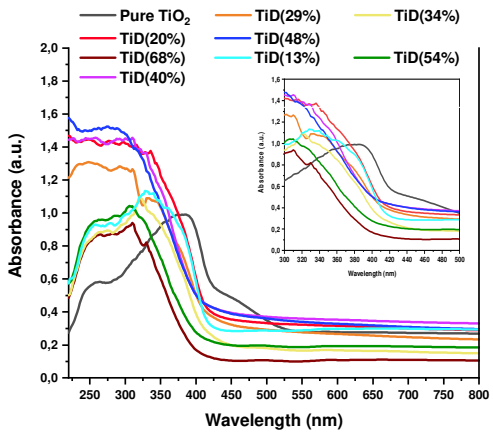

Fig. 11 The UV-Vis diffuse absorption spectra of all composite (DTi(SiO2 wt%) and pure TiO_2

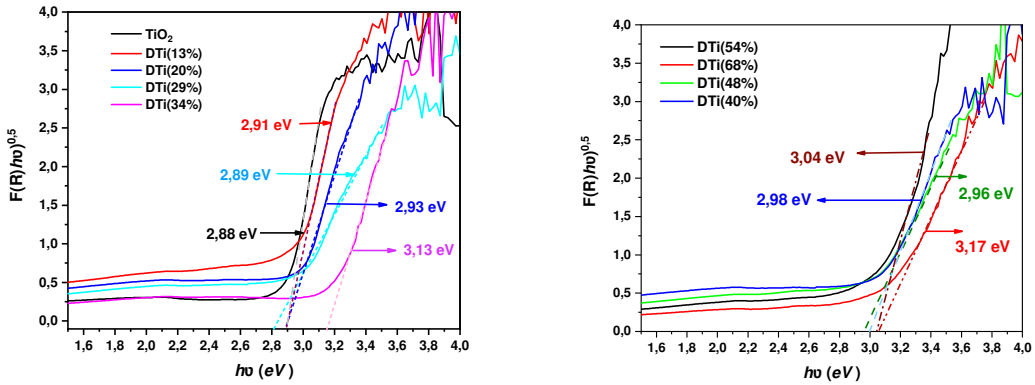

Fig. 12 the plots of transformed Kubelka-Munk function versus the energy of light ($h\nu$) for composite containing (a)less and (b)more than 34 wt% SiO_2 content in diatomite

Photocatalytic activity and adsorption

To evaluate the photocatalytic performance and adsorption capacity of synthesized composites with different diatomite loading, MDMA solution (10 mg/L) was tested at a dosage of 1g/L of the photocatalyst for a period of 2 hours under UV irradiation (368 nm) and constant agitation. In parallel, a same experiment was carried out in the absence of light to evaluate the adsorption capacity of samples during 150 min.

From Figures 13-17, it can be seen that, in the case of no irradiation (dark condition), the rate removal of MDMA is only of 10 % for pure TiO_2 and increases to 40 % for TiO_2/Dt(48%) composite after 60 min, which proves that the composites with higher TiO_2 loading (small amount of diatomite) have a lower adsorption capacity for MDMA. These results suggest also that the MDMA adsorption increases with increasing specific surface area and pore volume (Fig. 12, 14,16, 17 and Table 2). The adsorption of MDMA with only diatomite was also tested and reached 38% after 120 min which corresponded to the maximum adsorption capacity of treated diatomite(Fig. 14).

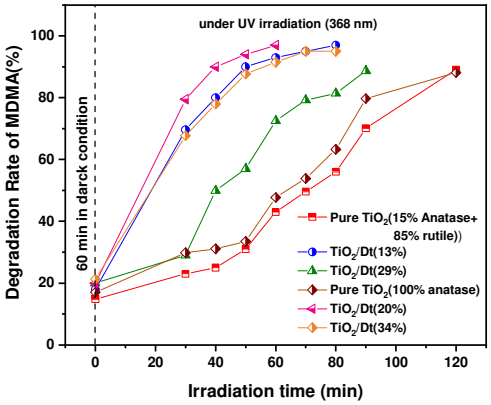

Fig. 13 Photocatalytic activity of Pure TiO_2 and composites prepared with small amount of diatomite (less than 34 wt.% SiO_2 content).

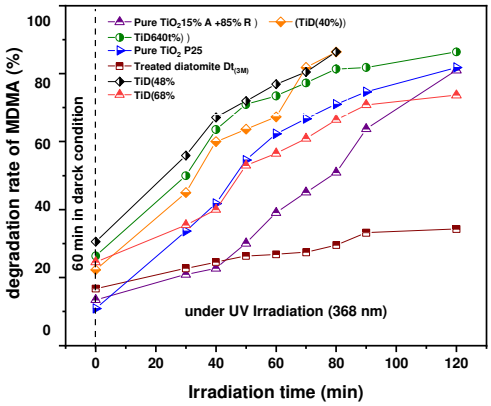

Fig. 14 Photocatalytic activity of composite containing single anatase TiO_2 phase (more than 34 wt.% SiO_2 content).

Fig. 15and Fig. 17 show the photocatalytic activity results obtained using composite prepared with small amount of diatomite and composite containing more than 34 wt.% of SiO_2 content respectively, compared to both prepared pure TiO_2 (85% rutile/15% anatase) and commercial TiO_2 Degussa P25 (20% rutile/80% anatase). The latter is taken as references because various researchers reported that TiO_2 P25 exhibited an excellent photocatalytic activity better than that of pure anatase phase [67, 68]. From our results (Figures 13, 14 and 15), it is clearly shown that the composites containing mixed phase and SiO_2 content ranging from 13-34 wt. % (Fig. 15 and 16) showed a better photocatalytic efficiency than all composites containing a single anatase phase (Fig. 14) and both TiO_2 P25 and prepared pure TiO_2, despite their lower surface area and adsorption capacity which indicates that the higher MDMA removal rate using this composite due mainly to the photodegradation process. This finding is due to the heterostructure anatase: rutile which inhibits the photogenerated electron/hole pair recombination and favored their separation [45] and lower and optimum SiO_2 coating (diatomite) which avoid the agglomeration of TiO2 NPs and improved the formation of hydroxyl radicals $OH^{\cdot}$ mainly came from the water adsorbed on the diatomite surface and composite.

Effect of SAA on adsorption/photodegradation

The results displayed on Table.2, Fig. 16 and Fig. 17 show that BET specific surface area (SAA) of prepared composite increased with increasing SiO_2 content in diatomite from 67 to 133 m^2/g until 48 wt.% of SiO2 which indicated that the adsorption capacity increased also with increasing SAA from 20 to 44% and achieved a maximum of adsorption after 150 min in dark condition when SiO_2 content is 48 wt.% due to its higher SAA, larger pore volume, smaller crystalline size of TiO_2 NPs and uniform dispersion of TiO_2 NPs on the surface of diatomite(fig.10) results the formation of mesopores between the TiO_2 nanoparticles and diatomite proved in fig.6 and fig.7, while when SiO_2 content in composite is more than 50 wt.% the SAA decreases to 87 and 104 m^2/g for TiD(54%) and TiD(68 %), respectively, compared to TiD(48%) probably due to the manner and the chap of immobilization of TiO_2 nanoparticles on the surface and in the pore of diatomite.

Among all, TiD(20%) appears to be the best composite for the photodegradation of MDMA with optimum TiO_2 loading (20% SiO_2 content) and anatase/rutile weight ratio of 58/42. The second best photocatalyst TiO_2/Dt(13%) is composed of the highest loading TiO_2 (39% anatase and 61% rutile). This result in agreement with previous research works in which it is reported that when the wt.% of SiO_2 added to TiO_2 ranged from 5 to 20 wt.%, the mixed oxide TiO_2/SiO_2 exhibited a higher photocatalytic efficiency compared to pure nano-TiO_2 prepared with different Ti and Si precursor [36,44,69,70].

Concerning the composite TiD(29%) with 63% of anatase, the photodegradation rate of MDMA is less important compared to TiD(34%) which contains 90 wt.% of anatase due to its low value of bad gap (2.89 eV) and strong absorption above 400 nm. After 60 min of irradiation, it can be observed from Fig. 15 that TiD(20%) achieved much higher photodegradation efficiency (98%). The decomposition rate of MDMA using the TiD(13%) and TiD(48%) composites were 93% and 90%, respectively, while TiD(29%) showed only 79% of decomposition, this can be explained by the presence of synergetic effect between the crystalline phase composition i.e. anatase/ rutile ratio and diatomite amount (SiO_2 content in composite).

Form Figures 12 and 13, it can be seen that when single anatase crystalline structure was formed without any trace of other crystalline phase (rutile and brookite), the composite TiD(48%) displayed the highest catalytic activity due to its largest surface area (133 m^2/g) and smallest TiO_2 crystallite size (5.5 nm) this result was confirmed by its highest light absorption in UV region (250-380nm) (fig.1 in supplementary data). A similar result was also reported by M. Riazian [71] who found that the composite SiO_2/TiO_2 containing lower than 45% of synthesized SiO_2 provided the maximum activity for methylene blue photodegradation. In addition, S. Nabih et al [72] and L. Zhou [73] have reported that the mixed oxide TiO_2/SiO_2 with amount ratio (1:1 wt ratio) showed the best activity. Moreover, the photodegradation rate reached 83% and 80% using TiDt(54%)and TiD(40%), respectively (Fig. 15), which proved that when SiO_2 content is more than 34 wt.% the photocatalytic activity increased with increasing surface area and pore volume (**Table. 2**), higher adsorption capacity and surface hydroxyl density (OH group at the surface of diatomite) [33]. All composites were more active than P25 and pure prepared TiO_2, except the TiD(68%) which showed the lowest activity (63%) but good adsorption capacity, due to the higher amount of diatomite which covered the surface of TiO_2 and leads to the decrease of photocatalytic efficiency. It was also found that when SiO_2 content is in excess in TiO_2 film a decrease in photocatalytic activity was observed due to the large band gap energy of SiO_2 (11 eV) [72]. Our results show clearly that the presence of diatomite (amorphous SiO_2 and some amount of quartz) improved the photocatalytic performance of TiO_2 NPs and adsorption capacity compared to pure TiO_2 but only until 53 wt.% of SiO_2 content in diatomite. This finding is in agreement with several literature studies which found that the addition of low content of synthesized SiO_2 to TiO_2 enhances the efficiency of SiO_2/TiO_2 composite materials [61].

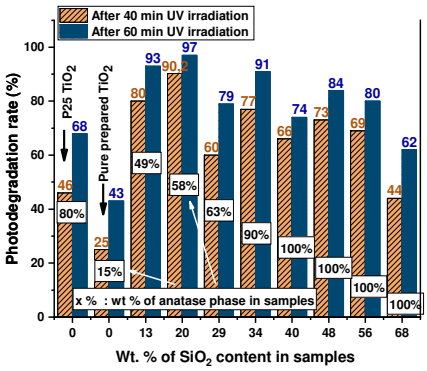

Fig 15. Effect of SiO_2 and anatase content on the photodegradation of MDMA after 40 and 60 min of UV irradiation (368 nm)

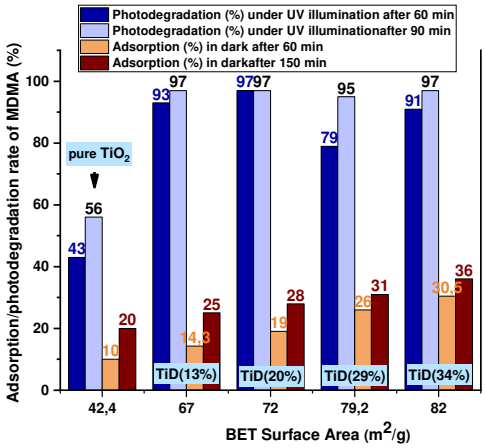

Fig. 16. Effect of the specific surface area (SAA) on MDMA adsorption and photodegradation of composite contained less than 34 wt.% of SiO_2

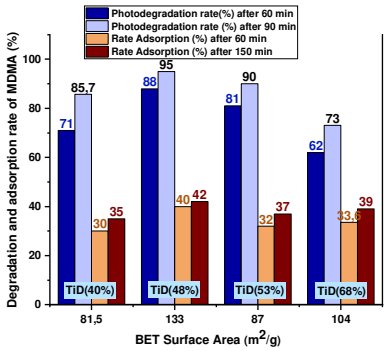

Fig. 17 Effect of the specific surface area on MDMA adsorption and photodegradation of composite contained more than 34 wt.% of SiO_2.

The reusability and stability of photocatalyst

The recycling performance of the best three composite DTi(13%), DTi(20%) and DTi(40%) has been evaluated in order to investigate their reusability and stability. The recycling performance of the best three composite DTi(13%), DTi(20%) and DTi(40%) has been evaluated in order to investigate their reusability and stability. The photodegradation of MDMA (10 mg/L) was evaluated for four cycles during 90 min under UV irradiation. After each cycle the composite was filtered and washed by ethanol and deionized water (3 times) then it was dried at 90 °C for 3 h before reused. As shown in Figure 18, the removal efficiency of the three composite kept almost constant even after four recycling tests. For the first run, 97% of MDMA degraded after 90 min using DTi(20%) composite ; subsequently, the rate degradation of second, third, and fourth run was 94 %, 90 %, and 82 %, respectively. In order to confirm the structural stability of the composites, XRD spectra of TDi(20%) and TDi(48%) solids which exhibited a good photocatalytic activity were recorded before and after four cycles (Fig.19). It can be observed from this figure that the crystalline structure of composite was maintained with just a slight decrease in intensity compared to the XRD spectra of starting composite due probably to the weight loss during washing and filtering process. These results (Fig.18 and 19) demonstrate that DTi(x%) composites have good reusability and stability in photodegrading MDMA and probably other similar organic pollutants. In addition the immobilization of TiO_2 NPs on diatomite surface facilitates and increases yield photocatalyst recovery from solution.

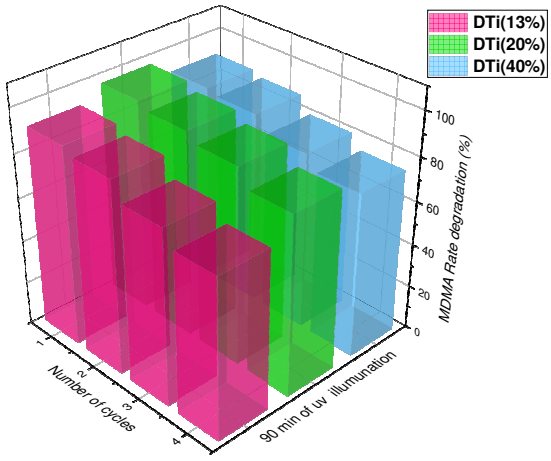

Fig.18 The reusability experiment results of MDMA degradation using DTi(13 %), DTi(20 %) and DTi(40 %)under UV-light irradiation.

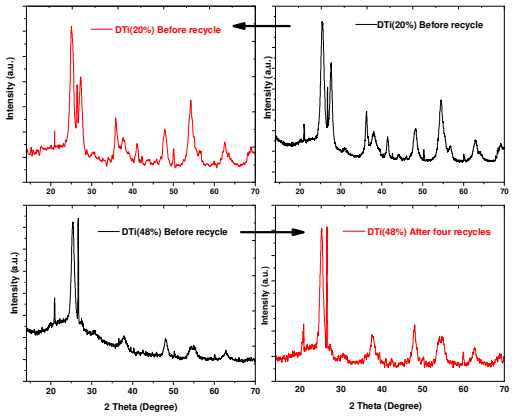

Fig.19 XRD Patterns of DTi(20 %) and DTi(40 %) composite before and after four cycles.

Conclusions

Titanium dioxide NPs were successfully synthesized by a facile sol-gel method on natural porous diatomite surface which has exceptionally high silica content. The uniform dispersion of TiO_2 Nps as confirmed by SEM image avoided their agglomeration and enhanced their photocatalytic activity.

The effect of diatomite on the formation of TiO_2 crystalline phases (rutile/anatase) was investigated. The results showed that when the content of SiO_2 added to TiO_2 is more than 34 wt % in TiO2/Diatomite composite, the formation of rutile was inhibited and only anatase phase was formed.

It may be concluded that the addition of diatomite has an important and significant effect on the crystalline phase formation, particles crystalline size, bad gap and surface area of TiO_2 which enhanced the adsorption of organic pollutants on its surface and improve its rate removal from wastewater.

The composite containing small amount of diatomite and mixed rutile/anatase phase exhibited the higher photocatalytic activity for degradation of Ecstasy due to the separation and lower recombination of photo-generated electron-hole pair through interface rutile/anatase and TiO_2/SiO_2 hetero-structure**.** The optimum composite which contains 20 wt. % of mixed amorphous SiO_2 and some amount of quartz silica in diatomite with anatase/rutile phase ratio of 58/42 removed 97% of MDMA in only 50 min.

Acknowledgements

The authors are grateful to the DGRSDT (Direction générale de la recherche scientifique et technique) of Algeria for research funding

Notes and references

1United Nations. World Drug Report (2019, 2020).https://www.unodc.org/wdr2019/and .https://wdr.unodc.org/wdr2020/

2 Y. Deng, C. Guo, H. Zhang, X. Yin, L. Chen, D. Wu and J. Xu, Environ. Sci. Eur., 2020, 32, 2-9

3 European Drug Report 2020: Trends and Development(EMCDDA)
https://www.emcdda.europa.eu/system/files/publications/2757/POD_Wastewater%20analysis_update2020.pdf
4 M. K.Yadav, M. D. Short, R. Aryal, C. Gerber, B.van den Akker, and C. P. Saint, *Water Res*., 2017, 124, 713–727.
5 P. K Thai, G. Jiang, W. Gernjak, Z. Yuan, F. Y. Lai, and J. F. Mueller, *Water Res.,* 2014, 48, 538–554.
6 A. K. McCall, R. Bade, J. Kinyua, , F. Y. Lai, P. K. Thai, A. Covaci and C. Ort, *Water Res*., 2016, 88, 933–947.
7 K. M Clauwaert, J. F. Van Bocxlaer and A. P. De Leenheer, *Forensic Sci. Int*., 2001, 124, 36–42.
8 B. Kasprzyk-Hordern, R. M. Dinsdale, A. J. Guwy, *Anal. Bioanal Chem,* 2008, 391, 1293–1308.
9 K. Paciuszkiewicz, M. Ryan, I. A.Wright, and J. K. Reynolds, *Water*., 2019, 11, 1071.
10 C. G. Daughton, Illicit Drugs in Municipal Sewage. In book: Pharmaceuticals and Personal Care Products in the Environment: Scientific and Regulatory Issues (pp.348-364). Edition: Symposium Series 791. Publisher: American Chemical Society: Washington, D.C. Editors: CG Daughton, TL Jones-Lepp. Author : Christian G Daughton
11 E. J. Rosi-Marshall, D. Snow, S. L. Bartelt-Hunt, A. Paspalof, J. L. Tank, *J. Hazard. Mater*., 2015, 282, 18–25.
12 C. F .Lin, Y. J. Shiu, C. S. Kuo, A. Y. C. Lin, C. H. Wu and P. K. A. Hong, *React. Kinet. Mech. Catal*., 2013, 110, 559–574.
13 S. Younis, and K. H. Kim,*Catal.*, 2020, 10, 1109.
14 Z.Zhuge ,X. Liu, Y.Gong, C.Li, L.Niu, S.Xu,X.Xu, Z. A .Alothman, C. Q.Sun, J. G.Shapter and Y.Yamauchi,*Chem. Eng. J.,* 2021, 421, 127838.
15 X.Liu, B.Liu, L. Li, Z. Zhuge, P.Chen, C.Li, Y.Gong,L.Niu, J. Liu, L.Lei, C.Q. Sun, *Appl. Catal. B*., 2019, 249 .82–90.
16 B .Liu, X. Liu, J. Liu, C.Feng, Z.Li, C. Li, Y.Gong, L.Pan, S. Xu,C.Q. Sun, *Appl. Catal. B* .,2018, *226, 234–241.*
17 X. Kang, S. Liu, Z. Dai, Y. He, X. Song and Z. Tan, *Catal*., 2019, 9, 191.
18 H. Dong, G. Zeng, L. Tang, C. Fan, C. Zhang and X. He, *Water Res*., 2015, 79, 128-146.
19. K. Nakata and A. Fujishima, *J. Photochem. Photobiol.*, 2012, 13, 169–189.
20 Y .Gong, Y. Wu,Y.Xu,L.Li,C. Li, X. Liu, L.Niu, *Chem. Eng. J*., 2018, 350, 257-267
21 M. Benčina , A. Iglič , M. Mozetič and I. Junkar, *Nanomaterials*., 2020 ,10,1121.
22 J. B. Chemin, S. Bulou, K. Baba, C. Fontaine, T. Sindzingre, N.D. Boscher and P. Choquet, *Scientific Reports*., 2018, 8, 9603.
23 T. L. Thompson and J. T. J. Yates, *Chem Rev*., 2006, 106, 4428–4453.
24 D. A. H. Hanaor and C. C. Sorrell , *J. Mater. Sci*., 2011, 46, 855–874.
25 T. Zhu and S.-P. Gao, S.-P., *J.Phys. Chem C., 2014, 118, 11385–11396.*
26 M. Besançon, L. Michelin, L. Josien, L. Vidal, K. Assaker, M. Bonne, B. Lebeau, J.L. Blin, *New J. Chem*., 2016, 40, 4386–4397.
27 B. Wang, F. C. de Godoi, S. Zheng, I. R. Gentlee and C. Li, *Powder Technol*., 2016, 302, 426–433.
28 G. Zhang, A. Peyravi, Z. Hashisho, Z. Sun, Y. Liu, S. Zhengb and L. Zhong, ***Catal. Sci. Technol.,*** 2020, **10**, 2378-2388
29 N. K. Boutoumi, H. Boutoumi, H. Khalaf, B. David, *Applied Clay Science*., 2013, 80–81 56-62.
30 M. Takeuchi, M. Hidaka, *J. Hazard. Mater.,* 2012, 237–238,133-139.
31 K. Kočí, V. Matějka, P. Kovář, Z. Lacný and L. Obalová, *Catal. Today.*, 2011, 161, 105-109.
32 S.N. Hosseini, S.M. Borghei, M. Vossoughi and N. Taghavinia, *Appl. Catal. B : Envir.,* 2007, 74, 53-62.
33 X. Zhao, W. Ju, J. Zhang, B. Liu, J.Zhanga and X. Yi, *New J. Chem*., 2019**,43**, 6234-6241.31.
34 M. Bellardita, M. Addamo, A. Di Paola, G. Marcì, L. Palmisano, L. Cassar and M. Borsa, M, *J. Hazard. Mater., 2010, 174, 707–713*
35 J.Wang, X. Liu, R. Li, P. Qiao, L. Xiao and J. Fan,*Catal. Commun*., 2012, 19, 96–99.
36 T. Ya. Datskoa and V. I. Zelentsova, *Surf. Eng. Appl. Electrochem.*, 2019, 55, 655–666.
37 B.Wang, G. Zhang, Z. Sun, S. Zhen, *Powder Technol*., 2014, 262, 1-8.
38 Y. Cheng, F. Luo, Y. Jiang, F. Li and C. Wei, *Colloids Surf. A Physicochem. Eng*., 2018, 554, 81-85.
39M. Kim, E.Park, H. Jung,S. T.Yun and J. Jurng,*Powder Technol*.,2014, 267, 153-160.
40 L. Xu , X. Gao , Z. Li and C. Gao, *Desalination*., 2015 369, 97–104.
41 T. Benkacem , B. Hamdi, A. Chamayou , H. Balard and R. Calvet,*Powder Technol.*, 2016, 294, 498-507.
42 M. Hirano, K. Ota and H. Iwata, *Chem. Mater.,* 2004, 16, 3725–3732.
43 A. Šuligoj, U. L.Štangar, A. Ristić, M. Mazaj, D. Verhovšek, and N. N. Tušar, *Appl. Catal. B Environ*., 2016,184, 119–131.
44 D. E. Rakhmawaty , S. N. Ishmah, M. D. Permana and M. L. Firdaus, *Catal*., 2020, 10, 1248.
45 B. Li, S. Wu, and X. Gao, A review, *Nanotechnol. Rev*., 2020, 9, 1080-1103.
46 J. Y. Hua, S. S. Zhang, Y. H. Cao, H. J. Wang, H. Yua and F. A .Peng, *ACS Sustainable Chem. Eng*., 2018, 6, 10823–10832.
47 A. Tiwari, I. Mondal, S. Ghosh, N. Chattopadhyay, U. Pal, *Phys. Chem. Chem. Phys*., 2016, 18, 15260–15268.
48 Z. Luo, A. S. Poyraz, C. H. Kuo, R. Miao, Y. T. Meng, S. Y .Chen, T. Jiang, C. Wenos and S. L. Suib, *Chem. Mater*., 2015, 67, 6–27.
49 W.Fu, , G. Li, Y. Wang, , S. Zeng, , Z. Yan, J. Wang and Z. Zhang, *Chem. Comm.,* 2018, 54, 58–61.
50 He, J., Du, Y., Bai, Y., An, J., Cai, X., Chen, Y., Feng, Q, *Molecules*., 2019, 24(16), 2996.
51 Q. Tay, X. Liu, Y. Tang, Z. Jiang, T. C. Sum, Z. Chen, *J. Phys. Chem* C., 2013, 117, 14973–14982.
52 L. Zhang, H. H. Mohamed, , R. Dillert, D. Bahnemann, : *A review. J. Photochem. Photobiol. C.,* 2012, 13, 263–276.
53 Y.Wei, M.V. Tokina, A. V. Benderskii, Z.Zhou, R. Long, and O. V. Prezhdo, *J. Chem. Phys*., 2020, 153, 044706.
54 N. S. Allen, N. Mahdjoub, V. Vishnyakov, P. J. Kelly and R. J.Kriek, *Polym. Degrad. Stab.*, 2018,150, 31–36.
55 H. WangX. Gao, G. Duan, X. Yang, X. Liu, *J. Environ. Chem. Eng*., 2015, 3, 603-608.
56 R. A. Spurr and H. Myers, *Analytical Chemistry.*, 1957, 29, 760-762.
57 S. Bakardjieva, , J. Šubrt, , V. Štengl, M. J. Dianez and M. J. Sayagues, *Appl. Catal. B.,* 2005, 58, 193–202.
58 B. Downs, R. Swaminathan and K. Bartelmehs, *American Mineralogist*., 1993, 78, 1104-1107.
59 G. S. Devi, K. A. S. Kumar and K. S. Reddy, *Particul. Sci. Technol.*, 2014 33, 219–223.

60 S. L. Isley and R. L. Penn, *J. Phys. Chem C.*, 2008, 112, 4469–4474
61 M. Andersson, L. Österlund, S. Ljungström, and A. Palmqvist, *J. Phys. ChemB.*, 2002, 106, 10674–10679.
62 D. M. Tobaldi , A. Tucci , A. S. Skapin and L. Esposito, *J. Eur. Ceram*. *Soc*., 2010, 30, 2481–2490.
63 H. Mahani, M. Kazemini, *Sci. Iran*., 2003 , 10 ,350 – 356
64 R. M. Rivera, B. Ulenaers, G. Ounoughene, K. Binnemans, T. V. Gerven, *Mine Eng*., 2018, 119, 82-92
65 J. C. P Broekhoff , *Stud. Surf. Sci. Catal.,* 1979, 3, 663–684.
66 Z. Sun, C. Bai, S. Zheng, X. Yang, Y. Xiaoping and R.L. Frost, *Appl. Catal. A*., 2013, 458 103–110.
67 T. Ishigaki, Y.Nakada, N.Tarutani, T.Uchikoshi, Y.Tsujimoto, M. Isobe , Hironori Ogata,C. Zhang and D. Hao, *R. Soc. open sci.,* 2020, 7, 191539.
68 F. Amano, M. Nakata, A. Yamamoto and T. Tanaka*, Catal. Sci. Technol*., 2016, 6, 5693-5699.
69 L. Sikong1, J. Damchan , K. Kooptarnond and S. Niyomwas, *J. Sci. Technol*., 2008, 30, 385-391.
70 M. Pierpaoli , X. Zheng , V. Bondarenko , G. Fava and M. L. Ruello, *Environments*., 2019, 6, 87.
71 M. Riazian, *JNS.*, 2014, 4, 433- 441.
72 S. Nabih, A. E. Shalan, E. S. A. Serea, M. A. Goda1 and M. F. Sanad, J*. Mater. Sci. Mater. Electron*.,2019, 30, 9623-9633.
73 L. Zhou, , S. Yan, B. Tian, , J. Zhang and M. Anpo, *Mater. Lett*., 2006, 60, 396–399.